Letter

# Cr-induced Perpendicular Magnetic Anisotropy and Field-Free Spin-Orbit-Torque Switching

T.C. Chuang,[1] C.F. Pai,[2] and S.Y. Huang[1,*]

[1] *Department of Physics, National Taiwan University, Taipei 10617, Taiwan*

[2] *Department of Materials Science and Engineering, National Taiwan University, Taipei 10617, Taiwan*

(Received 2 January 2019; revised manuscript received 19 April 2019; published 20 June 2019)

Current-induced spin-orbit torque (SOT) driven magnetization switching has relied mostly on 4*d* and 5*d* heavy metals with strong spin-orbit coupling to generate large spin currents to deliver SOT and a MgO layer to acquire perpendicular magnetic anisotropy (PMA). We demonstrate 3*d* Cr metal can generate PMA and deliver SOT switching with more prowess than Ta. In certain Cr-based heterostructures, even field-free SOT switching has been achieved due to the subtle microstructure in the layered structure. The field-free SOT switching device based on 3*d* Cr provides significant advantages for next generation high-efficiency and low-cost nonvolatile spintronic devices.

DOI: 10.1103/PhysRevApplied.11.061005

Recently, current switching of a ferromagnetic (FM) layer via spin-orbit torque (SOT) has drawn a great deal of interest for spintronic devices [1,2]. An FM layer, sandwiched between a heavy metal (HM) with strong spin-orbit coupling (SOC) and MgO, can acquire perpendicular magnetic anisotropy (PMA). When a lateral charge current $J_e$ flows through a HM/FM/MgO structure, the spin Hall and/or the Rashba effects generate a spin current $J_s$ through the FM layer with PMA and switch its magnetization via the SOT [3–5]. However, this highly attractive current-switching scheme occurs only if an external field is also applied along $J_e$, and its direction dictates the up and down orientations of the PMA layer. The external field is necessary to break the up-down degeneracy, but such a field is technologically unattractive. Spintronic applications demand field-free SOT switching. There are a few approaches to achieve field-free switching including the fabrication of geometrically asymmetric layers [6–10], the use of exchange bias via an antiferromagnetic layer [11–13], and other more complex schemes [14–18].

Previously, one most often employs HM layers of either 5*d* (e.g., Pt, W, and Ta) or 4*d* elements (e.g., Mo), for PMA and SOT switching to exploit the stronger SOC, hence a higher charge-to-spin conversion efficiency [4,10,19,20]. In this work, we show that 3*d* Cr layers can also induce strong PMA and deliver SOT switching, and most interestingly, field-free SOT switching. Previously, both HM and MgO have been essential for achieving PMA in HM/(Co, Fe)B/MgO heterostructures [2]. In contrast, the PMA in Cr-based heterostructures can be realized, even enhanced, without the MgO layer. Furthermore, we show that sputtering deposition induces oblique columnar growth in the layer structure, which induces an effective in-plane anisotropy for field-free switching. The direction of the oblique columnar structure dictates the up and down orientations of the PMA layer. Our results of SOT switching in 3*d* Cr-based heterostructures with unique advantages provide promising platforms for high-density and low-cost spintronic devices.

We use magnetron sputtering to grow Cr-based heterostructures including Ta(3)/CFB(1)/MgO(2)/Cr(1), Cr(3)/CFB(1)/MgO(2)/Cr(1), and Cr(3)/CFB(1)/Cr(0.5) on $Si/SiO_2$, where CFB = $Co_{60}Fe_{20}B_{20}$ is a common material for spintronic devices, and the thickness in nanometers is shown in the parentheses. After deposition, the multilayers are annealed in vacuum at 250 °C to acquire the interfacial PMA of the CFB layer. X-ray reflectivity and atomic force microscopy are used to determine film thickness and roughness. The magnetic properties are characterized by a vibrating sample magnetometer (VSM).

Previously, one has employed HMs of 4*d* and 5*d* elements to exploit their strong SOC, and thus spin Hall effect (SHE), for SOT switching, but not 3*d* metals. However, while some 3*d* metals, (e.g., Cu) have weak SHE, others (e.g., permalloy) have sizable SHE [21]. Unique among the 3*d* metals, Cr has very strong SHE, comparable to those in Pt and Ta, as has been demonstrated by spin pumping [22] and the spin Seebeck effect [23]. The SOT effective field of Cr has also been studied by second-harmonic measurement [24,25]. Here, we report deterministic field-free SOT switching in Cr-based heterostructures with robust PMA.

The multilayer structure of underlayer/CFB/capping layer is shown in Fig. 1(a), where the CFB layer acquires

*syhuang@phys.ntu.edu.tw

 

PMA when sandwiched between an underlayer (such as Cr as shown, or Ta) and a capping layer (Cr or Ta). Both Cr and Ta have negative spin Hall angles. The hysteresis loops of Ta/CFB/MgO/Ta, Ta/CFB/MgO/Cr, and Cr/CFB/MgO/Cr, measured by VSM with a magnetic field applied perpendicular and parallel to the film plane, are shown in Fig. 1(b). The sample of Ta/CFB/MgO/Ta shows PMA as previously known. However, we have also observed PMA in Ta/CFB/MgO/Cr, where Cr replaces Ta as the capping layer, and even in Cr/CFB/MgO/Cr, where Cr is both the underlayer and the capping layer. These results show Cr can induce robust PMA whose strength can be measured by the anisotropy field ($H_a$). In each case, the loops with in-plane field and perpendicular field merge at the anisotropy field ($H_a$), which is about 3500 and 3000 Oe for the Cr underlayer (bottom figure) and the Ta underlayer (middle figure), respectively. The magnetic anisotropy energy density of PMA can be estimated by $K_{\rm eff}t_{\rm FM} = (1/2)\mu_0 m_s H_a$, where $t_{\rm FM}$ is the FM layer thickness, $\mu_0$ is the vacuum permeability, and $m_s$ is the saturation magnetic moment per area [26]. The value of $K_{\rm eff}t_{\rm FM}$ for Ta/CFB/MgO/Cr is 0.06 erg/cm$^2$, whereas the value of 0.14 erg/cm$^2$ for Cr/CFB/MgO/Cr is much larger, demonstrating the prowess of Cr in establishing PMA.

We pattern the multilayers into Hall bar structures with widths of 10 $\mu$m for the electrical measurements. Figure 1(c) shows the anomalous Hall effect (AHE) resistance ($R_H$) as a function of out-of-plane magnetic field ($H_z$). The $R_H$ is defined by the Hall voltage divided by the applied current. We find that the measured $R_H$ of 2.6 Ω does not depend on the capping layers, but its value reduces to 1.8 Ω when the underlayer is Cr. The AHE loops of these heterostructures show a sharp transition and good squareness. The coercivity of about 16 Oe for Cr/CFB/MgO/Cr is larger than the other two samples with Ta at about 5 Oe.

We then employ current-induced SOT to switch the PMA CFB layer in these heterostructures containing Cr and Ta. As shown in Fig. 2(a), with the presence of an applied magnetic field $H_x$ along the current ($I$) direction, all devices can achieve deterministic switching with the same polarity, which confirms the same (negative) sign of the spin Hall angle for Cr and Ta. The Cr-based PMA samples exhibit a hysteresis $R_H$-$I$ loop with a higher squareness and a sharper switching behavior, in agreement with the AHE results. Thus, we unambiguously demonstrate SOT switching from the 3$d$ Cr layer without any HM. The critical current densities for the three heterostructures are comparable and remain unchanged with larger $H_x$. The value for Ta/CFB/MgO/Ta is $8.6 \times 10^6$ A/cm$^2$, which reduces to $4.9 \times 10^6$ A/cm$^2$ in Ta/CFB/MgO/Cr, but increases to $14.5 \times 10^6$ A/cm$^2$ in Cr/CFB/MgO/Cr, similar to the changes in the PMA anisotropy.

To quantitatively measure the SOT efficiency, we further perform current-induced hysteresis loop shift measurement [27]. This is illustrated in Fig. 2(b) for Ta/CFB/MgO/Ta, where the center of the AHE loop shifts to the positive

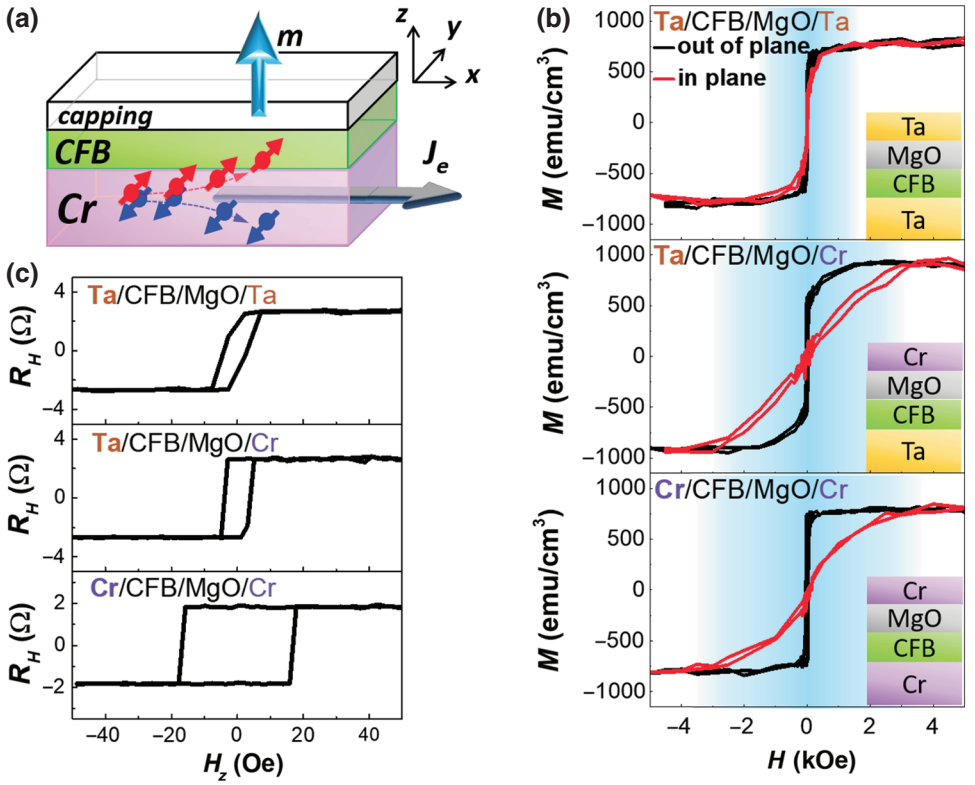


FIG. 1. (a) Schematic of the Cr-induced SOT by applying current ($J_e$) in a heterostructure with perpendicular magnetization ($m$). (b) The magnetic hysteresis loop with out-of-plane and in-plane magnetic field in the Ta/CFB/MgO/Ta, Ta/CFB/MgO/Cr, and Cr/CFB/MgO/Cr heterostructures. (c) Anomalous Hall resistance ($R_H$) as a function of out-of-plane magnetic field ($H_z$).

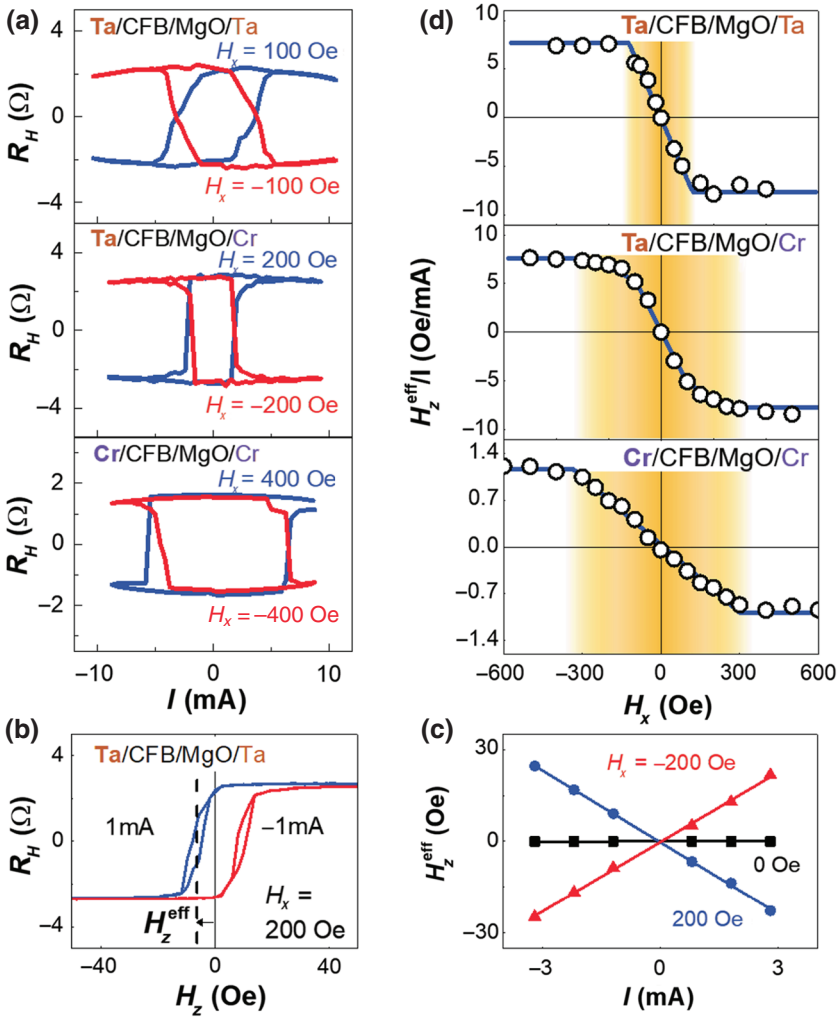


FIG. 2. (a) The current-induced switching with external in-plane magnetic field ($H_x$) along the electric current in the Ta- and Cr-based heterostructures. (b) The hysteresis loops measured with $H_x = 200$ Oe for Ta-based heterostructure with $I = \pm 1$ mA. $H_z^{\text{eff}}$ is defined by the damping-like SOT effective field. (c) $H_z^{\text{eff}}$ as a function of applied $I$ with $H_x = 0, \pm 200$ Oe. (d) $H_z^{\text{eff}}/I$ as a function of $H_x$ for the Ta- and Cr-based heterostructures.

(negative) direction by applying negative (positive) current of $I = 1$ mA in the presence of $H_x = 200$ Oe. This horizontal shift is induced by the damping-like SOT effective field ($H_z^{\text{eff}}$) along the out-of-plane direction, which scales linearly with the applied current, as shown in Fig. 2(c). Note that the sign of the linear slope and the shift of the $R_H$-$H_z$ loop reverses when the magnetic domain wall chirality is flipped by the opposite $H_x$. However, without $H_x$, there is no SOT-assisted domain expansion or contraction, resulting in zero $H_z^{\text{eff}}$. When $H_x$ is larger than the Dzyaloshinskii-Moriya interaction (DMI) effective field ($H_{\text{DMI}}$) at the interface, the domain wall starts to move along the preferred directions to achieve switching. On the other hand, $H_z^{\text{eff}}$is always proportional to $I$ for each different $H_x$, and the slope saturates to $H_{z(\text{sat})}^{\text{eff}}/I$ when $H_x \geq H_{\text{DMI}}$, as shown in Fig. 2(d). Here, the damping-like SOT efficiency $\xi_{\text{DL}}$ can be estimated by

$$\xi_{\text{DL}} = \frac{2e}{\hbar}\mu_0 m_s \frac{2}{\pi}\left(\frac{H_{z(\text{sat})}^{\text{eff}}}{I}\right)\left(\frac{\rho_{\text{CFB}} t_{\text{NM}} + \rho_{\text{NM}} t_{\text{CFB}}}{\rho_{\text{CFB}} t_{\text{NM}}}\right). \quad (1)$$

In Eq. (1), we include the shunting effect of metallic layers [28]. For the heterostructure with a Ta underlayer, despite different capping layers of Ta and Cr, the obtained $|\xi_{\text{DL}}|$ of $8.2 \times 10^{-2}$ and $8.8 \times 10^{-2}$ are comparable, while the value for the heterostructure with the Cr underlayer is much reduced at $1.1 \times 10^{-2}$. The obtained values of $H_{\text{DMI}}$ for Ta/CFB/MgO/Ta, Ta/CFB/MgO/Cr, and Cr/CFB/MgO/Cr are 115, 260, and 300 Oe, respectively. Apparently, Cr enhances $H_{\text{DMI}}$ in addition to $H_a$. Note that a further investigation is required to understand the microscopic origin of the enhanced $H_{\text{DMI}}$, including the Heisenberg exchange interaction, the orbital anisotropy, and the degree of the inversion symmetry breaking at the interface [29–32]. It is known that a Néel-type domain wall induced by DMI is the key to achieve SOT switching [33,34]. We estimate the strength of the DMI by $|D| = \mu_0 M_s \sqrt{A/K_{\text{eff}}} H_{\text{DMI}}$ [35], where $D$ is the DMI exchange constant, $M_s$ is the saturation magnetization per unit volume, $A$ is the exchange stiffness constant around $1.5 \times 10^{-11}$ J/m [36], and $K_{\text{eff}}$ is defined before. The obtained value of $|D| \sim 0.11$ mJ/m$^2$ in Ta/CFB/MgO/Ta is consistent with previous reports [37].

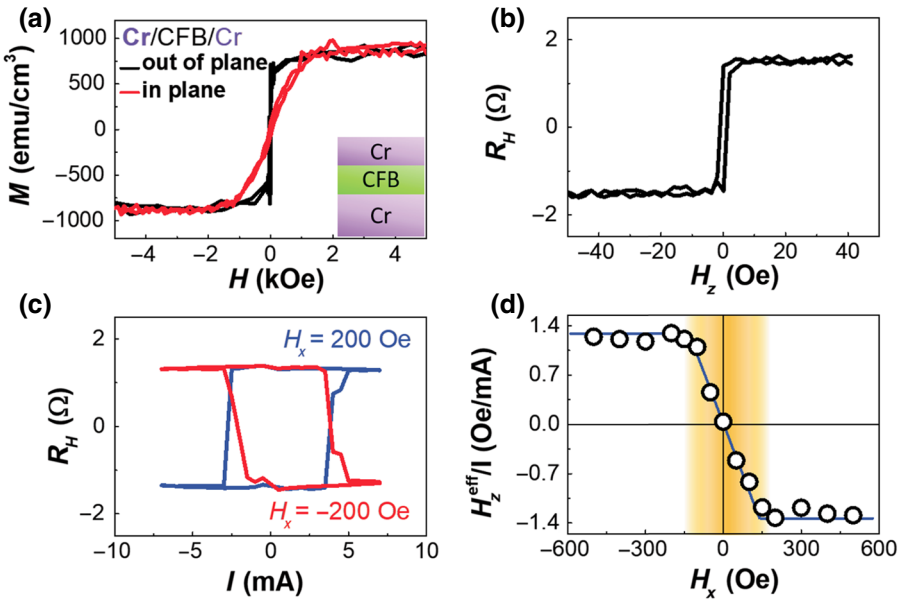


FIG. 3. Results of (a) the magnetic hysteresis loop with out-of-plane and in-plane magnetic field. (b) The $R_H$ as a function of $H_z$. (c) The current-induced switching as a function of $H_x$. (d) $H_z^{\text{eff}}/I$ as a function of $H_x$ for the Cr/CFB/Cr heterostructure.

We find a significantly higher value of $|D| \sim 0.25$ mJ/m$^2$ in Cr-based heterostructures.

Another remarkable feature of Cr is that the interfacial PMA can be formed in the Cr/CFB/Cr heterostructure even without the MgO layer. As shown in Fig. 3(a), a strong PMA with $H_a = 1600$ Oe and $K_{\text{eff}}t_{\text{FM}} = 0.07$ erg/cm$^2$ can exist in Cr(3)/CFB/Cr(0.5). This may be associated with the high enthalpy of oxide formation of the capping Cr layer [38,39]. Furthermore, the coercivity in the AHE loop is significantly reduced to 1 Oe, as shown in Fig. 3(b), which is beneficial to reduce the critical current density in SOT switching. As shown in Fig. 3(c), the obtained value of $6.0 \times 10^6$ A/cm$^2$ for critical switching current density without the MgO layer is about two times smaller than that with the MgO layer. In addition, from the current-induced hysteresis loop shift measurement in Fig. 3(d), $H_{\text{DMI}}$ and $|D|$ are about 150 Oe and 0.19 mJ/m$^2$, respectively, which indicates the presence of a stable Néel wall. On the other hand, $|\xi_{\text{DL}}|$ is slightly increased to $1.4 \times 10^{-2}$ compared with Cr/CFB/MgO/Cr.

After demonstrating the deterministic SOT switching in Cr, we further achieve the highly desirable field-free switching by exploiting the slanted columnar structure in thin film at different locations on the substrate. The geometrical relation between the substrate plate situated at 53 mm above the 2-inch sputtering gun is shown in Fig. 4(a). We pattern devices made from samples at various locations on the substrate plate at different horizontal distances ($x'$) from the center, which is directly above the center of the sputtering source. In Fig. 4(b), the thickness within $|x'| < 7$ mm is uniform, which can also be confirmed by the consistent value of $R_H$ within the same range. While the film is uniform, each of these locations at a different $x'$ has a different tilt angle ($\beta$) with respect to the vertical direction, where $\beta = 0$ at $x' = 0$, as shown in Fig. 4(c). We then conduct SOT current switching measurement without a magnetic field for these samples, anticipating that no switching will take place. This is indeed the case for samples with $x' \approx 0$, $\beta \approx 0°$, such as the results with $\beta \approx 1°$ shown in Fig. 4(d). However, at larger $\beta$, partial switching appears, and at $\beta \geq 7°$, we have accomplished field-free SOT switching for both Ta/CFB/MgO/Cr and Cr/CFB/MgO/Cr. Interestingly, the critical switching current remains the same in these cases. One notes that the inability of, the propensity for, and the accomplishment of field-free switching is determined entirely by the location of the sample on the substrate. The SOT switching polarity is reversed when samples are measured at locations with negative $\beta$, as shown in Fig. 4(d). These results rule out oxidation, magnetic anisotropy gradient, and slight layer thickness differences as possible causes [6,7,40].

Instead, we investigate the microstructure of the cross-sections of films by the field emission gun scanning electron microscope (FEG SEM). We find clear evidences of a tilted columnar structure whose orientation directly correlates with the oblique angle deposition and the shadowing effect during sputtering deposition. As a consequence, the in-plane isotropy has been broken, with an in-plane symmetric axis in place acting as the role of an applied magnetic field in SOT switching. The evidence of tilted columnar microstructure is clearly observed in Fig. 4(e), when Ta films of 300-nm thickness grow at different positions along $x'$ axis by sputtering. The oblique columnar growth is a general phenomenon and occurs in all sputtered materials including amorphous, single crystalline, and polycrystalline films [41,42]. The sign of $\beta$ can be

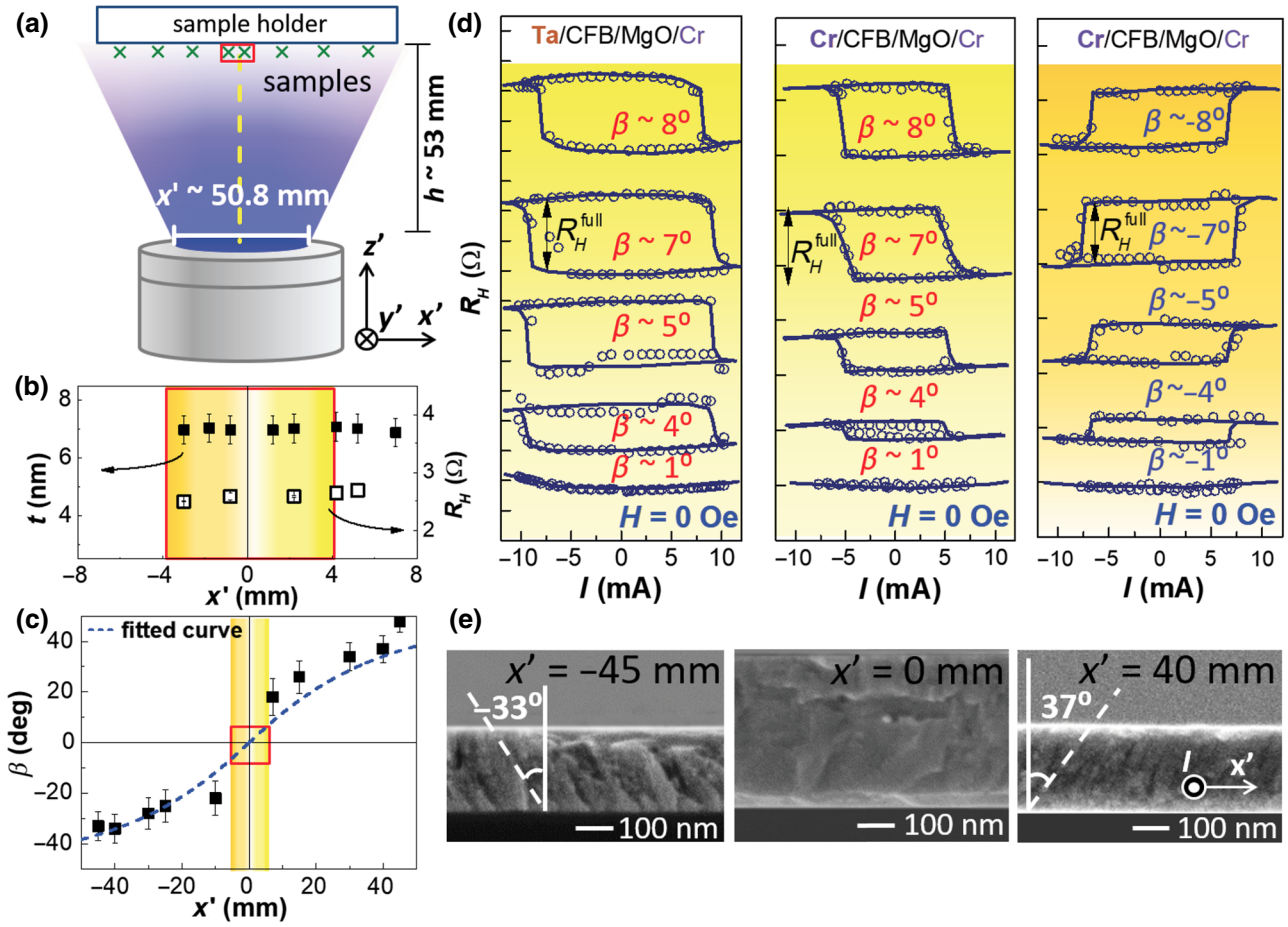


FIG. 4. (a) Schematic diagrams of sputtering deposition. The thickness and $R_H$ of sample and the tilt angle $\beta$ of columnar structure as a function of deposition position in (b),(c). The dash line in (c) is fitted by the cosine rule. (d) The current-induced switching without external magnetic field measured at different positions as shown in the red block marked area in (b),(c) for both the Ta- and Cr-based heterostructures. The solid lines of the current switching loops are guided by eyes. (e) Cross-section FEG SEM images of Ta films grown by sputtering at different positions ($x' = -45$, 0, and 40 mm).

changed when the samples locate at two sides of the center position. In Fig. 4(c), we show $\beta$ as a function of position $x'$. $\beta$ increases with the value of $x'$ and can be well described by the cosine rule [43] with only one fitting parameter, $h$, the distance between gun to sample holder, as

$$\beta = \tan^{-1}\frac{x'}{h} - \sin^{-1}\left(\frac{\{1-\cos[\tan^{-1}(x'/h)]\}}{2}\right). \quad (2)$$

We find good agreement between the calculated value of $h = 51.4$ mm with the actual one. From the fitting curve result of Fig. 4(c), we estimate the critical angle $\beta$ to have the field-free deterministic SOT switching around $5° \pm 1°$. Therefore, when the mirror symmetry along the $x'$ axis is broken by slanted columnar thin films with a slightly tilted angle, the corresponding current-induced SOT can facilitate magnetization switching. We suggest the zero-field current-induced switching can be accomplished via the effective in-plane field associated with spin-transfer torque [44]. The direction of the current and the tilting columnar microstructure need to be orthogonal to each other. On the other hand, the SOT switching cannot occur when the charge current flows along the $x'$ direction. This finding provides a significant path toward field-free SOT switching and has a strong impact for films prepared by sputtering.

In summary, we unambiguously demonstrate $3d$ Cr can induce strong interfacial PMA, SOT switching, and even field-free SOT switching. By utilizing the Cr layer alone, without heavy metals and a MgO layer, the robust PMA provides an attractive way to explore high-efficiency current-induced SOT and ultra-low damping spintronic devices. Importantly, we realize field-free SOT switching and find the underlying cause of the slanted columnar structure in the otherwise uniform thin films. This oriented columnar structure breaks the in-plane isotropy and facilitates field-free magnetic switching. Our results shed light on field-free SOT switching and uncover the significant

role of 3*d* materials with a variety of functions for next generation spintronic devices.

## ACKNOWLEDGMENTS

We thank C. L. Chien from Johns Hopkins University and D. Qu from Academia Sinica for valuable discussions. We also thank Professor C.S. Lin and Ms. Y.T. Lee from Instrumentation Center, National Taiwan University for FEG SEM experiments. This work was supported by the Ministry of Science and Technology of Taiwan, under Grants No. MOST 106-2628-M-002-015-MY3 and No. 105-2112-M-002-007-MY3. This work was also partially supported by Academia Sinica and National Taiwan University. S.Y.H. acknowledges support from the Golden Jade Fellowship from the Kenda Foundation, Taiwan.

[1] T. Wang, J. Q. Xiao, and X. Fan, Spin–orbit torques in metallic magnetic multilayers: Challenges and new opportunities, Spin **07**, 1740013 (2017).

[2] B. Dieny and M. Chshiev, Perpendicular magnetic anisotropy at transition metal/oxide interfaces and applications, Rev. Mod. Phys. **89**, 025008 (2017).

[3] I. M. Miron, K. Garello, G. Gaudin, P. J. Zermatten, M. V. Costache, S. Auffret, S. Bandiera, B. Rodmacq, A. Schuhl, and P. Gambardella, Perpendicular switching of a single ferromagnetic layer induced by in-plane current injection, Nature **476**, 189 (2011).

[4] L. Liu, C.-F. Pai, Y. Li, H. W. Tseng, D. C. Ralph, and R. A. Buhrman, Spin-torque switching with the giant spin hall effect of Tantalum, Science **336**, 555 (2012).

[5] J. Kim, J. Sinha, M. Hayashi, M. Yamanouchi, S. Fukami, T. Suzuki, S. Mitani, and H. Ohno, Layer thickness dependence of the current-induced effective field vector in Ta|CoFeB|MgO, Nat. Mater. **12**, 240 (2013).

[6] G. Yu, P. Upadhyaya, Y. Fan, J. G. Alzate, W. Jiang, K. L. Wong, S. Takei, S. A. Bender, L. T. Chang, Y. Jiang, M. Lang, J. Tang, Y. Wang, Y. Tserkovnyak, P. K. Amiri, and K. L. Wang, Switching of perpendicular magnetization by spin-orbit torques in the absence of external magnetic fields, Nat. Nanotechnol. **9**, 548 (2014).

[7] G. Yu, L.-T. Chang, M. Akyol, P. Upadhyaya, C. He, X. Li, K. L. Wong, P. K. Amiri, and K. L. Wang, Current-driven perpendicular magnetization switching in Ta/CoFeB/[TaOx or MgO/TaOx] films with lateral structural asymmetry, Appl. Phys. Lett. **105**, 102411 (2014).

[8] L. Youa, O. Leea, D. Bhowmika, D. Labanowskia, J. Honga, J. Bokora, and S. Salahuddin, Switching of perpendicularly polarized nanomagnets with spin orbit torque without an external magnetic field by engineering a tilted anisotropy, Proc. Natl. Acad. Sci. U.S.A. **112**, 10310 (2015).

[9] C. K. Safeer, E. Jue, A. Lopez, L. Buda-Prejbeanu, S. Auffret, S. Pizzini, O. Boulle, I. M. Miron, and G. Gaudin, Spin-orbit torque magnetization switching controlled by geometry, Nat. Nanotechnol. **11**, 143 (2016).

[10] T.-Y. Chen, H.-I. Chan, W.-B. Liao, and C.-F. Pai, Current-Induced Spin-Orbit Torque and Field-Free Switching in Mo-Based Magnetic Heterostructures, Phys. Rev. Appl. **10**, 044038 (2018).

[11] Y. W. Oh, S. H. Chris Baek, Y. M. Kim, H. Y. Lee, K. D. Lee, C. G. Yang, E. S. Park, K. S. Lee, K. W. Kim, G. Go, J. R. Jeong, B. C. Min, H. W. Lee, K. J. Lee, and B. G. Park, Field-free switching of perpendicular magnetization through spin-orbit torque in antiferromagnet/ferromagnet/oxide structures, Nat. Nanotechnol. **11**, 878 (2016).

[12] S. Fukami, C. Zhang, S. DuttaGupta, A. Kurenkov, and H. Ohno, Magnetization switching by spin-orbit torque in an antiferromagnet-ferromagnet bilayer system, Nat. Mater. **15**, 535 (2016).

[13] A. van den Brink, G. Vermijs, A. Solignac, J. Koo, J. T. Kohlhepp, H. J. Swagten, and B. Koopmans, Field-free magnetization reversal by spin-Hall effect and exchange bias, Nat. Commun. **7**, 10854 (2016).

[14] Q. Ma, Y. Li, D. B. Gopman, Y. P. Kabanov, R. D. Shull, and C. L. Chien, Switching a Perpendicular Ferromagnetic Layer by Competing Spin Currents, Phys. Rev. Lett. **120**, 117703 (2018).

[15] X. Wang, C. Wan, W. Kong, X. Zhang, Y. Xing, C. Fang, B. Tao, W. Yang, L. Huang, H. Wu, M. Irfan, and X. Han, Field-free programmable spin logics via chirality-reversible spin-orbit torque switching, Adv. Mater. **30**, e1801318 (2018).

[16] J. M. Lee, K. Cai, G. Yang, Y. Liu, R. Ramaswamy, P. He, and H. Yang, Field-free spin-orbit torque switching from geometrical domain-wall pinning, Nano Lett. **18**, 4669 (2018).

[17] S. C. Baek, V. P. Amin, Y. W. Oh, G. Go, S. J. Lee, G. H. Lee, K. J. Kim, M. D. Stiles, B. G. Park, and K. J. Lee, Spin currents and spin-orbit torques in ferromagnetic trilayers, Nat. Mater. **17**, 509 (2018).

[18] W. Chen, L. Qian, and G. Xiao, Deterministic current induced magnetic switching without external field using giant spin hall effect of beta-W, Sci. Rep. **8**, 8144 (2018).

[19] L. Liu, O. J. Lee, T. J. Gudmundsen, D. C. Ralph, and R. A. Buhrman, Current-Induced Switching of Perpendicularly Magnetized Magnetic Layers Using Spin Torque From the Spin Hall Effect, Phys. Rev. Lett. **109**, 096602 (2012).

[20] C.-F. Pai, L. Liu, Y. Li, H. W. Tseng, D. C. Ralph, and R. A. Buhrman, Spin transfer torque devices utilizing the giant spin Hall effect of tungsten, Appl. Phys. Lett. **101**, 122404 (2012).

[21] B. F. Miao, S. Y. Huang, D. Qu, and C. L. Chien, Inverse Spin Hall Effect in a Ferromagnetic Metal, Phys. Rev. Lett. **111**, 066602 (2013).

[22] C. Du, H. Wang, F. Yang, and P. C. Hammel, Systematic variation of spin-orbit coupling withd-orbital filling: Large inverse spin Hall effect in 3d transition metals, Phys. Rev. B **90**, 140407(R) (2014).

[23] D. Qu, S. Y. Huang, and C. L. Chien, Inverse spin Hall effect in Cr: Independence of antiferromagnetic ordering, Phys. Rev. B **92**, 020418(R) (2015).

[24] Z. Wen, J. Kim, H. Sukegawa, M. Hayashi, and S. Mitani, Spin-orbit torque in Cr/CoFeAl/MgO and Ru/CoFeAl/MgO epitaxial magnetic heterostructures, AIP Adv. **6**, 056307 (2016).

[25] B. Cui, S. Chen, D. Li, J. Yun, X. Guo, K. Wu, X. Zhang, Y. Wang, Y. Zuo, M. Gao, and L. Xi, Current-induced magnetization switching in Pt/Co/Ta with interfacial decoration by insertion of Cr to enhance perpendicular magnetic anisotropy and spin-orbit torques, Appl. Phys. Express **11**, 013001 (2018).

[26] M. T. Johnson, P. J. H. Bloemen, F. J. A. d. Broeder, and J. J. d. Vries, Magnetic anisotropy in metallic multilayers, Rep. Prog. Phys. **59**, 1409 (1996).

[27] C.-F. Pai, M. Mann, A. J. Tan, and G. S. D. Beach, Determination of spin torque efficiencies in heterostructures with perpendicular magnetic anisotropy, Phys. Rev. B **93**, 144409 (2016).

[28] T.-Y. Chen, C.-T. Wu, H.-W. Yen, and C.-F. Pai, Tunable spin-orbit torque in Cu-Ta binary alloy heterostructures, Phys. Rev. B **96**, 104434 (2017).

[29] H. T. Nembach, J. M. Shaw, M. Weiler, E. Jué, and T. J. Silva, Linear relation between Heisenberg exchange and interfacial Dzyaloshinskii-Moriya interaction in metal films, Nat. Phys. **11**, 825 (2015).

[30] A. Kundu and S. Zhang, Dzyaloshinskii-Moriya interaction mediated by spin-polarized band with Rashba spin-orbit coupling, Phys. Rev. B **92**, 094434 (2015).

[31] A. Belabbes, G. Bihlmayer, F. Bechstedt, S. Blugel, and A. Manchon, Hund's Rule-Driven Dzyaloshinskii-Moriya Interaction at 3d-5d Interfaces, Phys. Rev. Lett. **117**, 247202 (2016).

[32] S. Kim, K. Ueda, G. Go, P. H. Jang, K. J. Lee, A. Belabbes, A. Manchon, M. Suzuki, Y. Kotani, T. Nakamura, K. Nakamura, T. Koyama, D. Chiba, K. T. Yamada, D. H. Kim, T. Moriyama, K. J. Kim, and T. Ono, Correlation of the Dzyaloshinskii-Moriya interaction with Heisenberg exchange and orbital asphericity, Nat. Commun. **9**, 1648 (2018).

[33] S. Emori, U. Bauer, S. M. Ahn, E. Martinez, and G. S. Beach, Current-driven dynamics of chiral ferromagnetic domain walls, Nat. Mater. **12**, 611 (2013).

[34] O. J. Lee, L. Q. Liu, C. F. Pai, Y. Li, H. W. Tseng, P. G. Gowtham, J. P. Park, D. C. Ralph, and R. A. Buhrman, Central role of domain wall depinning for perpendicular magnetization switching driven by spin torque from the spin Hall effect, Phys. Rev. B **89**, 024418 (2014).

[35] A. Thiaville, S. Rohart, É Jué, V. Cros, and A. Fert, Dynamics of Dzyaloshinskii domain walls in ultrathin magnetic films, Europhys. Lett. **100**, 57002 (2012).

[36] A. Conca, J. Greser, T. Sebastian, S. Klingler, B. Obry, B. Leven, and B. Hillebrands, Low spin-wave damping in amorphous $Co_{40}Fe_{40}B_{20}$ thin films, J. Appl. Phys. **113**, 213909 (2013).

[37] J. Torrejon, J. Kim, J. Sinha, S. Mitani, M. Hayashi, M. Yamanouchi, and H. Ohno, Interface control of the magnetic chirality in CoFeB/MgO heterostructures with heavy-metal underlayers, Nat. Commun. **5**, 4655 (2014).

[38] B. Rodmacq, A. Manchon, C. Ducruet, S. Auffret, and B. Dieny, Influence of thermal annealing on the perpendicular magnetic anisotropy of Pt/Co/AlOx trilayers, Phys. Rev. B **79**, 024423 (2009).

[39] M. W. Chase, enthalpy. *NIST-JANAF Themochemical Tables, Fourth Edition, J. Phys. Chem. Ref. Data, Monograph* **9**, 1 (1998).

[40] Y. Zhang, S. Luo, X. Yang, and C. Yang, Spin-orbit-torque-induced magnetic domain wall motion in Ta/CoFe nanowires with sloped perpendicular magnetic anisotropy, Sci. Rep. **7**, 2047 (2017).

[41] A. Barranco, A. Borras, A. R. Gonzalez-Elipe, and A. Palmero, Perspectives on oblique angle deposition of thin films: From fundamentals to devices, Prog. Mater. Sci. **76**, 59 (2016).

[42] R. Álvarez, L. González-García, P. Romero-Gómez, V. Rico, J. Cotrino, A. R. González-Elipe, and A. Palmero, Theoretical and experimental characterization of $TiO_2$thin films deposited at oblique angles, J. Phys. D: Appl. Phys. **44**, 385302 (2011).

[43] R. N. Tait, T. Smyb, and M. J. Bretta, Modelling and characterization of columnar growth in evaporated films, Thin Solid Films **226**, 196 (1993).

[44] S. Fukami, T. Anekawa, C. Zhang, and H. Ohno, A spin-orbit torque switching scheme with collinear magnetic easy axis and current configuration, Nat. Nanotechnol. **11**, 621 (2016).